AIP | Review of Scientific Instruments

An electron energy loss spectrometer designed for studies of electronic energy losses and spin waves in the large momentum regime

H. Ibach, J. Rajeswari, and C. M. Schneider

Citation: Rev. Sci. Instrum. **82**, 123904 (2011); doi: 10.1063/1.3670731
View online: http://dx.doi.org/10.1063/1.3670731
View Table of Contents: http://rsi.aip.org/resource/1/RSINAK/v82/i12
Published by the American Institute of Physics.

An electron energy loss spectrometer designed for studies of electronic energy losses and spin waves in the large momentum regime

H. Ibach,[1,3] J. Rajeswari,[2,3,a)] and C. M. Schneider[2,3]
[1]*Peter Grünberg Institut (PGI-3), Forschungszentrum Jülich, 52425 Jülich, Germany*
[2]*Peter Grünberg Institut (PGI-6), Forschungszentrum Jülich, 52425 Jülich, Germany*
[3]*Jülich Aachen Research Alliance - Fundamentals of Future Information Technologies (JARA-FIT), 52425 Jülich, Germany*

(Received 13 May 2011; accepted 29 November 2011; published online 21 December 2011)

Based on 143° electrostatic deflectors we have realized a new spectrometer for electron energy loss spectroscopy which is particularly suitable for studies on surface spin waves and other low energy electronic energy losses. Contrary to previous designs high resolution is maintained even for diffuse inelastic scattering due to a specific management of the angular aberrations in combination with an angle aperture. The performance of the instrument is demonstrated with high resolution energy loss spectra of surface spin waves on a cobalt film deposited on the Cu(100) surface. © *2011 American Institute of Physics*. [doi:10.1063/1.3670731]

I. INTRODUCTION

Many techniques for surface analysis make use of electrons as probing particles. Devices for electron energy analysis have therefore always played an important role in the methodology of surface science. This paper concerns a spectrometer with electrostatic deflector type devices for studies on inelastic electron scattering. The experimental technique is known as *electron energy loss spectroscopy* or *high resolution electron energy loss spectroscopy*. The method has been used predominantly for surface vibration spectroscopy,[1] more recently however also for the spectroscopy of surface plasmons[2–5] and surface spin waves (magnons).[6–10] The various applications of the technique are reviewed in Ref. 11. The most successful energy loss spectrometers use a special free-form electrostatic deflector introduced in 1993.[12] This deflector features stigmatic focusing at a deflection angle of about 143° as well as angular aberration correction for small angles in the dispersion plane. Contrary to the spherical deflector stigmatic focusing is achieved not by the (spherical) symmetry but rather by deflection. The deflector can therefore carry larger electron currents and is thus particularly useful for the production of monochromatic electron beams of high intensity. Spectrometers with this type of deflectors, both as monochromators and as analyzers, have demonstrated surface vibration spectra with a resolution below 1 meV (Ref. 13) and are commercially available.

For studies on surface electronic transitions and surface spin waves, less resolution is required however in combination with high currents to compensate for the small signals. A spectrometer for spin-polarized electrons was described in Ref. 14 and has been successfully used in several applications.[6–10] To achieve the spin polarization vertical to the scattering plane a special combination of a 90° deflector with a 180° deflector was used for electron monochromatization. Later, a theoretical study showed that seven times higher currents could be achieved by a combination of two 143°-deflectors as monochromators.[15]

We have constructed a spectrometer on the basis of two 143°-deflectors as monochromators and analyzers each with enlarged entrance and exit slits of the deflectors. The spectrometer indeed exhibited higher currents for energy resolutions above 10 meV compared to previous designs. However, we found the resolution to degrade dramatically when electrons backscattered from surfaces were studied. The degrading is the more severe, the higher the contribution from diffuse scattering is. The present paper is concerned with the origin of the degradation effect which is pertinent also to spectrometers of previous designs when operated in the range of low resolution and low impact energies. It is shown that the effect is caused by the angular aberrations of the electrostatic deflectors in combination with the absence of explicit angle apertures. The resolution degradation can be avoided by shifting the angular aberrations of the analyzer from the plane perpendicular to the dispersion plane into the dispersion plane (see Secs. III and V for details) and by adding an angle aperture for angles in the dispersion plane. The performance of the new instrument is demonstrated with electrons backscattered from a sample and with high resolution spectra (7 meV) on the surface spin waves of fcc cobalt films for momentum transfer along the [011] direction.

II. THE SPECTROMETER

Our electron spectrometer features a thermal cathode emission system (LaB_6-cathode), two 143°-deflectors in sequence as monochromators, a lens system between monochromators and sample, a second identical, however reversed lens system, and a double-pass analyzer consisting of two 143°-deflectors and the channeltron detector (Fig. 1). All elements of the spectrometer are designed with the help of trajectory calculations following the principles outlined in Ref. 16. Within the monochromator section the space charge produced by the large current loads is taken into account. The lens system possesses C_{2v} rather than circular symmetry to

a)Electronic mail: r.jayaraman@fz-juelich.de.

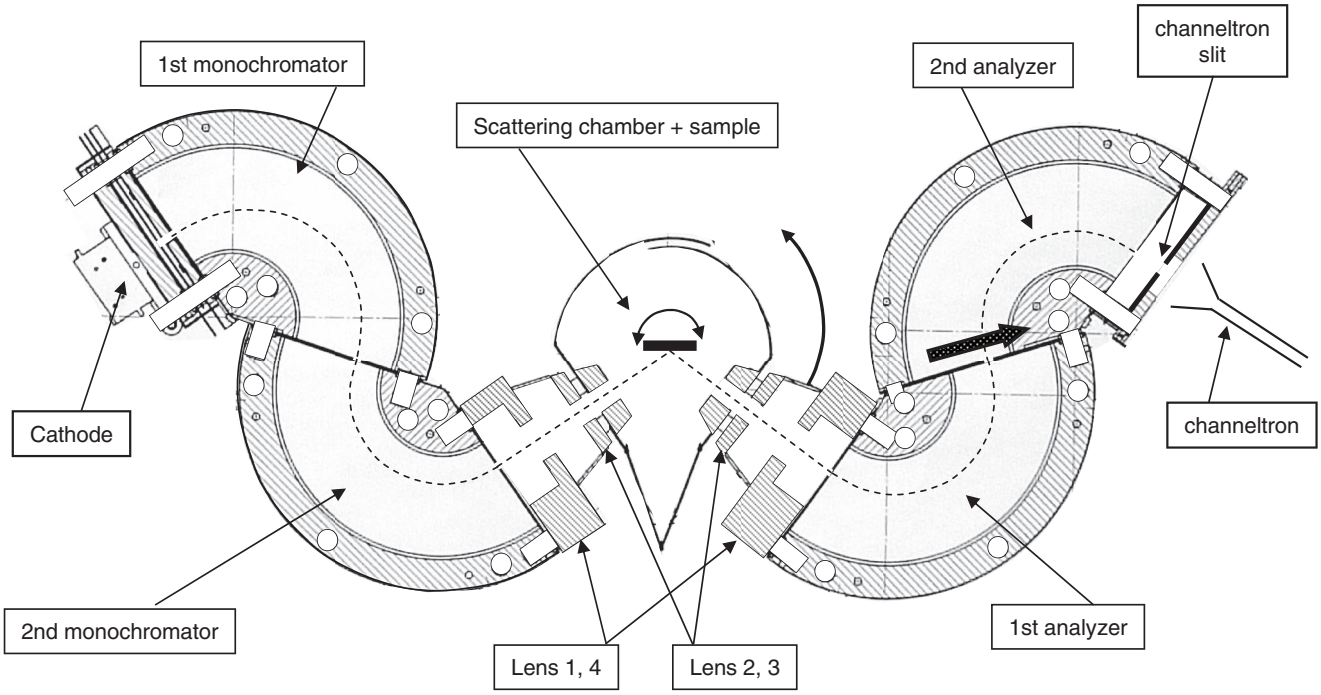

FIG. 1. The electron spectrometer featuring a thermal cathode emission system, two 143°-deflectors in sequence as monochromators, a lens system between monochromators and sample, a second identical, however reversed lens system, and a double-pass analyzer consisting of two 143°-deflectors and the channeltron detector. The dashed line very roughly illustrates the central path of the electron trajectories. In the final version of the spectrometer the analyzer operates with a larger central radius of the trajectories. See text for further details.

realize different focusing in and perpendicular to the spectrometer plane (as shown in Fig. 1). The spectrometer differs from the design used in surface vibration spectroscopy mainly in the dimensions of the entrance and exit slits of the deflectors (0.6 mm × 6 mm instead of 0.3 mm × 3 mm), the different radial positions of the entrance and exit slit in the first monochromator and by the addition of a second deflector analyzer. Further differences are discussed in Sec. VI. The larger slits serve to increase the monochromatic current at moderate resolution. The shift in the radial position of the entrance and exit slit in the first monochromator (see Fig. 1) serves to have the beam entering the second monochromator in the direction orthogonal to the slit plane under the high current loads of interest here (up to 10 μA).

The geometry and the equipotential contours of the 143°-deflectors used here are shown in Fig. 2. The deflector may be considered as a variant of a cylindrical deflector with equipotential plates carrying the entrance and exit slits and additional top and bottom cover plates.[16] The negative potential on those plates ("compression voltage") provides for equipotential lines that are curved similar to a spherical deflector (Fig. 2(d)) which yields a stigmatic image of the entrance slit at the position of the exit slit for a particular compression voltage and a particular total deflection angle. The specific deflector used here possesses radii $r_i = 20.3$ mm and $r_a = 60.3$ mm of the inner and outer deflection plates. Entrance and exit slits are placed at the radial position $r_0 = 33.5$ mm and the radius of the concave curvature is $r_c = 100$ mm. For those dimensions stigmatic focusing is achieved at a total deflection angle $\theta_{tot} = 143.8°$.

The stigmatic focusing of the device is demonstrated with the electron trajectories in Fig. 3. Panel (a) displays calculated trajectories $r(\theta) = r_0 + y(\theta)$ in the dispersion plane for electrons emerging at the center of the entrance slit at $r(\theta) = r_0$, i.e., at $y(\theta) = 0$. The entrance angles with respect to the normal on the entrance slit are $\alpha = -4°, -2°, 0°, +2°$, and $+4°$. As seen from the figure the radial position $r(\theta)$ does not stay near r_0 but rather rises up to 40 mm in the center of the device even for $\alpha = 0°$. Panel (b) shows trajectories $z(\theta)$ in the plane orthogonal to the dispersion plane emerging again at the center of the entrance slit. The entrance angles with respect to

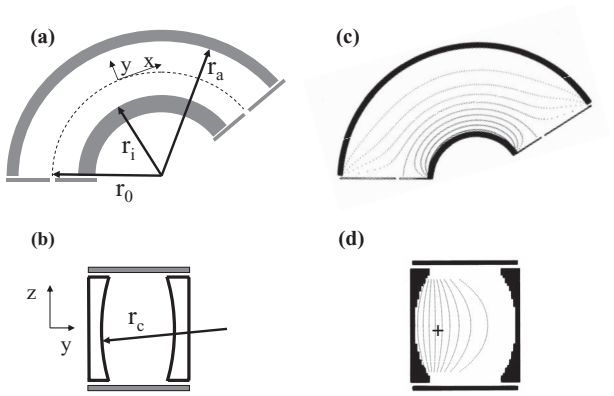

FIG. 2. Free-form electrostatic deflector that features stigmatic focusing, equipotential metal apertures and a correction of the angular aberration in the dispersion plane:[12] (a) cross section in the dispersion plane showing the deflector plates and the entrance and exit apertures; (b) cross section perpendicular to the electron path showing the concavely shaped deflector plates; (c) and (d) as (a) and (b), yet with the dashed equipotential lines obtained from the solution of the Laplace-equation for the device. The cross in (d) marks the radial position of the slits.

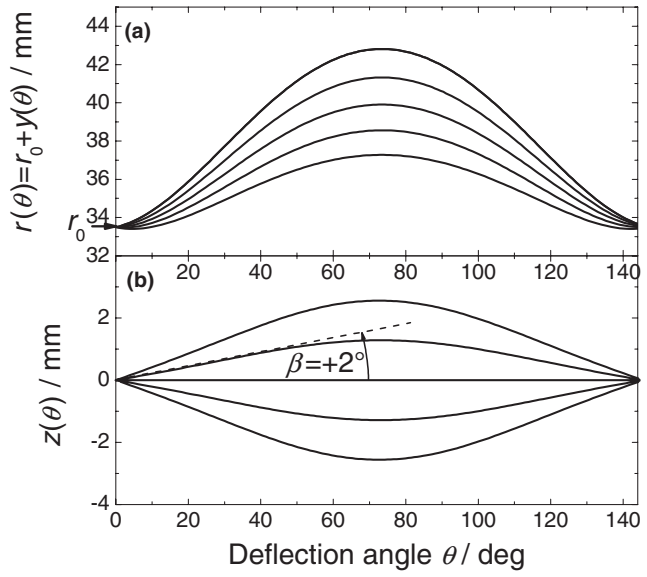

FIG. 3. Electron trajectories in the 143°-deflector of the type shown in Fig. 2 as a function of the deflection angle θ. Parameters are the radial position of the entrance slit $r_0 = 33.5$ mm, radii of inner and outer deflection plate $r_i = 20.3$ mm and $r_o = 60.3$ mm, respectively, and $r_c = 100$ mm. (a) Trajectories within the dispersion plane ($(r(\theta), \theta)$-plane, as shown in Fig. 1) emerging in the center of the entrance slit at r_0. Entrance angles with respect to the normal on the entrance slit are $\alpha = -4°, -2°, 0°, 2°$, and 4°. (b) Trajectories $z(\theta)$ perpendicular to the dispersion plane for the entrance angles $\beta = -4°, -2°, 0°, 2°$, and 4°.

the normal on the entrance slit are $\beta = -4°, -2°, 0°, +2°$, and $+4°$.

The pass energy of the deflector E_{pass} depends mainly on the ratio of r_a and r_i. As for the ideal cylindrical field the pass energy is proportional to the voltage difference ΔU between the outer and inner deflection plate and to $\ln^{-1}(r_a/r_i)$. While the pass energy of an ideal cylindrical field $E_{pass,\,cyl}$ is

$$E_{pass,cyl} = \frac{\Delta U}{2\ln(r_a/r_i)}, \tag{1}$$

the pass energy of the 143°-deflector with the dimensions specified above is

$$E_{pass} = 1.18 E_{pass,cyl}. \tag{2}$$

The potential of entrance and exit slits U_{slit} is set equal to the mean potential of the inner and outer deflection plates denoted as U_i and U_o, respectively,

$$U_{slit} = \frac{(U_i + U_o)}{2}. \tag{3}$$

The performance of spectrometers is usually characterized by the current in "*direct beam*" at the detector for a given overall resolution. *Direct beam* means the sample is removed from the scattering chamber and the analyzer is rotated so that the monochromatic electron beam aims directly into the analyzer. The lens potentials are optimized to obtain maximum current in the detector. The value of the *direct beam current* as a figure of merit is limited, however. What eventually counts are current and resolution obtained in actual experiments, i.e., after scattering from a surface. In this regard, the present spectrometer was a disappointment initially. This is demonstrated with Fig. 4. The left panel (a) displays the *direct beam* current measured at the entrance of the channeltron multiplier as function of energy. The electron energy in the scattering chamber is 6.8 eV. The deflection voltages in the first and second monochromators are $\Delta U = 4.84$ V and $\Delta U = 2.88$ V, respectively, and the deflection voltages of both analyzers are $\Delta U = 2.88$ V. Panel (b) displays the spectrum of electrons after specular reflection from a Cu(100) surface at an angle of 48° measured from the surface normal. All electrode potentials are set as for Fig. 4(a). Now, the full width at half maximum (FWHM) of the elastic peak has increased by more than a factor of three and the spectrum has developed a tail on the high energy side.

A clue to the origin of the resolution degradation seen here is provided by the observation that the smaller the sharper the mirror reflex (i.e., the better the long range order) of the surface is, the lower the FWHM is. This suggests that the energy broadening is caused by electrons having embarked on trajectories with larger angles with respect to the optical axis and therefore enter the analyzer at large angles α and β with respect to the normal on the entrance slit, much larger than shown in Fig. 3. In other words the degradation of the resolution is attributed to the angle aberrations of the

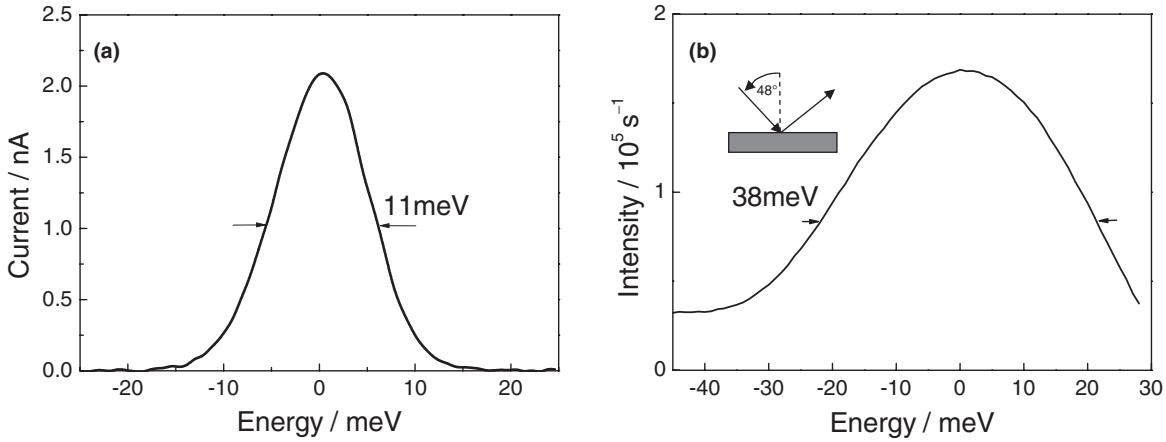

FIG. 4. (a) Current measured at the channeltron entrance as function of energy when the monochromatic beam is directly viewed with the analyzer ("direct beam"). (b) Elastic peak after specular reflection from a clean Cu(100) sample. Kinetic energy at the sample was 6.8 eV and the scattering angle was 48° from the surface normal. The full width at half maximum is dramatically broadened and the spectrum displays a tail on the high energy side.

143°-deflector. A further hint to the same origin is that the FWHM can be reduced by applying modified lens voltages. This is the procedure followed with the 90°/180° spectrometer located in Halle.[17] However, the count rate in the spectra is then far from being optimal since the solid angle of diffuse scattering that is accepted by analyzer lens and analyzer as well as the overall transmission is lower. For a particular potential setting used with the 90°/180° spectrometer in a recent study[9] we calculate a reduction by an order of magnitude.[18] To develop a better solution for the problem we need to discuss the angular aberrations of the 143°-deflector.

III. ANGULAR ABERRATION OF THE 143°-DEFLECTOR

Angle aberrations of the deflector analyzer are best discussed with the help of the image equation in the dispersion plane which relates the deviations of the radial coordinate from the center of the entrance slit $y_{\text{entr}} = y(\theta = 0°)$ to the corresponding coordinate in the exit slit $y_{\text{exit}} = y(\theta = 143.8°)$ (see also Fig. 3). This image equation reads

$$y_{\text{exit}} = -y_{\text{entr}} + D\frac{\delta E}{E_{\text{pass}}} - c_{\alpha\alpha}\alpha^2 - c_{\beta\beta}\beta^2. \quad (4)$$

Here, D is the dispersion, δE is the deviation from the pass energy E_{pass}, and $c_{\alpha\alpha}$ and $c_{\beta\beta}$ are the aberration coefficients for the entrance angles α and β defined as before, respectively. First order terms in α and β vanish because of the focus in the exit slit. For an ideal spherical deflector one has $c_{\alpha\alpha} = 2r_0$ with r_0 the radius of the center path and $c_{\beta\beta} = 0$ because of the azimuthal symmetry of the sphere. By virtue of the concave curvatures of the deflection plates (Fig. 2(b)) $c_{\alpha\alpha}$ is reduced. The smaller the radius of curvature r_c, the smaller is $c_{\alpha\alpha}$. The sum of the aberration coefficients $c_{\alpha\alpha} + c_{\beta\beta}$ stays constant, however.[12] Usually, the concave curvature is chosen such as to make $c_{\alpha\alpha} = c_{\beta\beta}$ since this choice yields the highest solid acceptance angle for electrons at pass energy.

We now study the transmission *versus* energy for the 143°-deflector for bundles of electrons with α, β angular spreads $\alpha_{\max} = \beta_{\max} = 3°$ and $\alpha_{\max} = \beta_{\max} = 10°$. Here and in the following, *transmission* is defined as the fraction of electrons entering the entrance slit that leaves the exit slit. The voltage difference on the deflection plates is $\Delta U = 1$ V, rendering a *pass energy* of $E_{\text{pass}} = 0.542$ eV. Technical details of the calculations are approximately as described in Ref. 16. The transmission curves in Fig. 5 are calculated with a bundle of 5000 electrons at each energy starting from a random position within the 0.6 mm × 6 mm entrance slit and at angles randomly chosen between $-\alpha_{\max} < \alpha < \alpha_{\max}$ and $-\beta_{\max} < \beta < \beta_{\max}$. For $\alpha_{\max} = \beta_{\max} = 3°$ the transmission curve is narrow and symmetric. The FWHM is $\Delta E_{1/2} = 4.3$ meV and the base width is $\Delta E_{\text{B}} = 13$ meV. The peak transmission of 0.72 differs from 1.0 mostly because of the fact that the image of the entrance slit at the exit slit position is curved. The transmission changes dramatically when $\alpha_{\max} = \beta_{\max} = 10°$. Now, the FWHM as well as the base width have increased by a factor of 4 ($\Delta E_{1/2} = 18.5$ meV, $\Delta E_{\text{B}} = 43$ meV). Moreover, the transmission curve takes an asymmetric shape with a long tail to the high energy side. The large increase of the FWHM

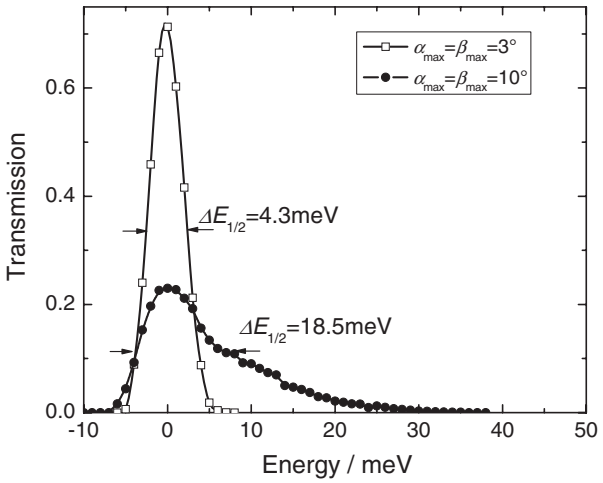

FIG. 5. Transmission *versus* energy of the 143°-deflector for a bundle of electrons with maximum angles $\alpha_{\max} = \beta_{\max} = 3°$ and $\alpha_{\max} = \beta_{\max} = 10°$ shown as open squares and solid circles, respectively. The zero of the energy is placed at the maximum of the transmission curves. Dimensions of the deflector are as noted in Fig. 2. Entrance and exit slits measured 0.6 mm × 6 mm. The deflection voltage is $\Delta U = 1$ V, rendering a pass energy of 0.54 eV.

and the base width is in accordance with the experimental observations in Fig. 4. The nearly quantitative agreement with experiment is fortuitous, of course, since the increase in the angular spread of the beam after reflection from a surface depends on the actual status of the surface. Nevertheless, we can safely conclude from the simulations that the degradation of the resolution observed in Fig. 4 is caused by electrons entering the analyzer at large angles α and/or β.

This conclusion raises two questions. First, why does the degradation of the resolution not occur in direct beam, and second, why is the degradation much lower for electron spectrometers used in high resolution vibration spectroscopy? The answer to the first question is straightforward. The currents in both monochromators are space charge saturated in the sense that the input current provided by the cathode emission system is set such that the peak current (current at the maximum of the transmission curve of the monochromators) has its maximum. Simulations that include the space charge of electrons show that under those circumstances only electrons with angles near the center path leave the exit slit. Hence, the monochromatic beam should have a small angular spread as an intrinsic property and therefore a narrow energy spread. The answer to the second question requires a more in-depth analysis. We have performed extensive studies on the electron trajectories with the lens system carrying the electrons from the monochromator to the analyzer via diffuse scattering at the sample. In particular, we have studied the width of the angle distribution of electrons entering the analyzer after diffuse scattering from the sample. For an impact energy at the sample of 5 eV we have studied pass energies of $E_{\text{pass}} = 0.5$ eV and $E_{\text{pass}} = 2.5$ eV. The lower pass energy would be typical for high resolution spectroscopy of surface vibrations. We found that for the low pass energy of 0.5 eV electrons possessing large angles with respect to the optical axis for the most part do not enter the analyzer. Rather their trajectories end on the plate outside the slit. On the other hand, for E_{pass}

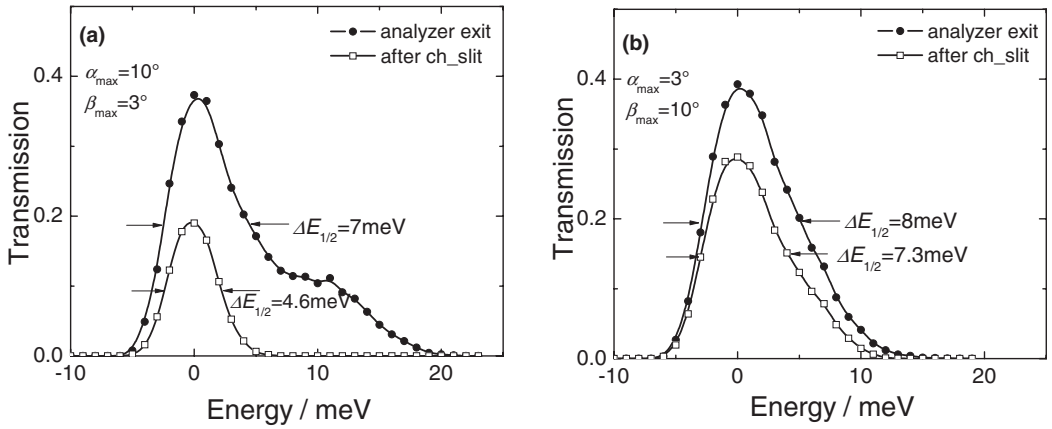

FIG. 6. Transmission curves of the 143°-deflector for a bundle of electrons with (a) $\alpha_{max} = 10°$, $\beta_{max} = 3°$ and (b) $\alpha_{max} = 3°$, $\beta_{max} = 10°$. All other parameters are as for Fig. 5. The solid circles mark the transmission curves for the analyzer *per se*. The open squares represent the transmissions after passing through a second slit at 10 mm distance measuring 1 mm × 6 mm.

= 2.5 eV a large fraction of electrons with high angles entered the analyzer. High resolution spectroscopy is therefore much less affected by the degradation effect. This is consistent with the experimental observations in surface vibration spectroscopy where one typically finds a resolution degradation of 20–30% after scattering from surfaces.

Conceivable strategies to avoid the adverse effect of large angles in the deflector could encompass (i) blocking large angle electrons from entering the analyzer, (ii) blocking them from being counted by the detector, or (iii) the use of analyzers that tolerate larger angles. For the 143°-deflector analyzer a combination of measures proved to be successful: We make use of the possibility to reduce the angular aberration coefficient $c_{\beta\beta}$ at the expense of a larger $c_{\alpha\alpha}$. The adverse effect of large α-angles is controlled by an angle aperture between analyzer and detector which blocks electrons with large α-angles from entering the channeltron detector.

IV. INTRODUCTION OF AN APERTURE FOR α-ANGLES

Because of the strategy described above the effect of large α- and β-angles on the resolution are to be considered separately. Figure 6 shows the transmission curves of the 143°-deflector for a bundle of electrons with (a) $\alpha_{max} = 10°$, $\beta_{max} = 3°$ and (b) $\alpha_{max} = 3°$, $\beta_{max} = 10°$. The deflection voltage ΔU is 1 V. Similarly all other parameters are as for Fig. 5. The solid circles mark the transmission curves for the analyzer *per se*. In both cases, for large α_{max} and large β_{max}, the transmission curves are significantly broadened in FWHM as well as in the base width and the curves tail towards the high energy side. The broadening, however, is more significant for large $\alpha_{max} = 10°$ (Fig. 6(a)). In this case there is even a hump in the tail at about +11 meV measured from the maximum. The hump in Fig. 5 is therefore to be attributed to large α-angles.

Electrons having embarked on trajectories with large α-angles are easily blocked from entering the detector by introducing a second slit (*channeltron slit*) between the analyzer exit and the detector (see also Fig. 1). We have studied different dimensions of this slit. The transmission curves with open squares in Fig. 6 represent the results for an optimized design which consists of a 1 mm × 6 mm slit placed at a distance of 10 mm behind the analyzer exit. The transmission with the slit in place (open squares in Fig. 6(a)) displays nearly the same FWHM as the transmission in Fig. 5 where both α_{max} and β_{max} were 3°. Scaled to the different spread in β-angles of the incoming beam the peak transmission in Fig. 6(a) is nearly as in Fig. 5 (Fig. 6(a): 0.19 × 10/3 = 0.63, Fig. 5: 0.71). The channeltron slit is therefore an effective block for electrons with large α-angles. The channeltron slit has little effect on the transmission curves for large β-angles, however (Fig. 6(b)).

V. REDUCTION OF THE β-ABERRATION OF THE 143°-DEFLECTOR

A smaller aberration coefficient $c_{\beta\beta}$ of the 143°-deflector can be achieved by enlarging the concave radii of the deflection plates (Fig. 2).[12] A particular simple method to reduce $c_{\beta\beta}$ (at the expense of a larger $c_{\alpha\alpha}$) on an already existing 143°-deflector is to place entrance and exit slits at a larger radial position. We have studied the transmission curves of the 143°-deflector for various radial positions of the slits and found an optimum around $r_0 = 41.5$ mm. The transmission curves for this slit position are illustrated in Fig. 7. Figure 7(a) shows the energy distribution for $\alpha_{max} = 10°$ and $\beta_{max} = 3°$ while Fig. 7(b) is for $\alpha_{max} = 3°$ and $\beta_{max} = 10°$. Due to the larger angular aberration in α the energy distribution in Fig. 7(a) is extremely broad (solid circles) unless the large α-angles are blocked by the channeltron slit (open squares). Large β-angles have practically no adverse effect on the resolution (Fig. 7(b)). Furthermore, the transmission curve stays symmetric even for large angles α and β.

VI. TECHNICAL REALIZATION AND PERFORMANCE

The simplest technical realization of a 143°-deflector analyzer with entrance and exit slits at $r_0 = 41.5$ mm is achieved by shifting the second analyzer in the spectrometer in the

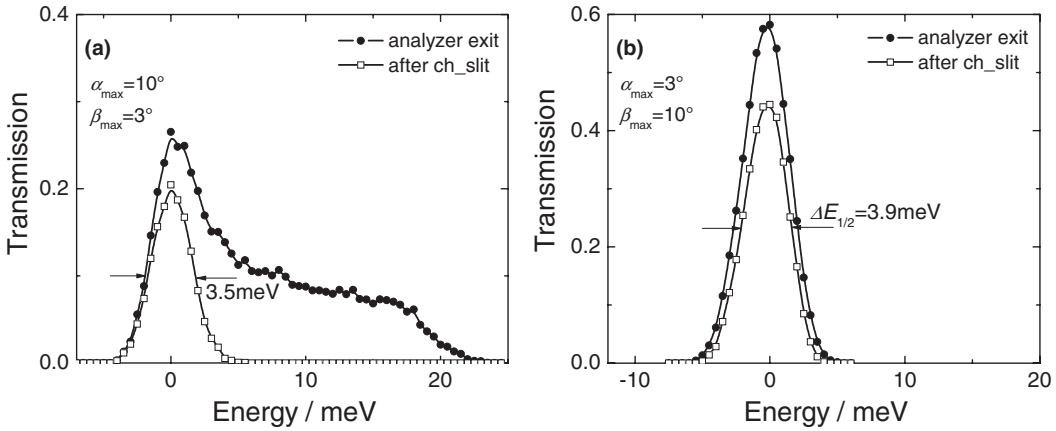

FIG. 7. Transmission curves of the 143°-deflector for a bundle of electrons with (a) $\alpha_{max} = 10°$, $\beta_{max} = 3°$ and (b) $\alpha_{max} = 3°$, $\beta_{max} = 10°$. The radial position of the slits is now at 41.5 mm. The solid circles mark the transmission curves for the analyzer *per se*. The open squares are the transmissions after passing through a second slit at 10 mm distance measuring 1 mm × 6 mm. The resolution hardly degrades for large β. Large angles α do not affect the resolution when they are cut off by the second slit (a).

direction along the dark shaded large arrow shown in Fig. 1 by 8 mm. The exit slit which is fixed to the first analyzer at a radius of $r_0 = 33.5$ mm thereby becomes an entrance slit of the second analyzer at $r_0 = 41.5$ mm. The exit slit of the second analyzer and the channeltron slit are replaced by new slits at $r_0 = 41.5$ mm.

As expected from the calculations, the spectrometer equipped with the modified second analyzer shows almost no degradation of resolution after the beam is reflected from a sample. Figure 8 compares the energy distribution as measured in direct beam (a) with the distribution after reflection from a Cu(100) sample (b). In both cases, the FWHM is about 14 meV. For a less well reflecting sample and when measuring energy distribution of the elastic diffuse scattering the FWHM increases moderately to 18 meV.

The experimental FWHM may be compared to the FWHM calculated from the simulations. The total FWHM is obtained by folding the product of the transmission curves of the two monochromators with the product of the transmission curves of the two analyzers. Since the transmission curves resemble Gaussians the total FWHM ΔE_{tot} can be calculated from the total FWHMs of the two monochromators ΔE_{mono} and the two analyzers ΔE_{ana} as

$$\Delta E_{tot} = \left(\Delta E_{mono}^2 + \Delta E_{ana}^2\right)^{1/2} \tag{5}$$

with

$$\Delta E_{mono,ana} = \Delta E_1 \Delta E_2 (\Delta E_1^2 + \Delta E_2^2)^{-1/2}. \tag{6}$$

For the deflection voltage of 4.5 V for the first monochromator and 3.0 V for the second monochromator and for the analyzers our simulation yields FWHM values of 18 meV, 14 meV, 14 meV, and 9.8 meV for the first monochromator, the second monochromator, and the two analyzers, respectively ($\alpha_{max} = \beta_{max} = 3°$). Using Eqs. (5) and (6) one calculates $\Delta E_{tot} = 13.7$meV in excellent agreement with the experimental data.

The performance of the spectrometer is further demonstrated with energy loss spectra of the surface spin waves on fcc cobalt films deposited on Cu(100) surfaces. The surface spin waves were first detected for wave vectors along the [011] direction ($\overline{\Gamma}\,\overline{X}$-direction)[6] using the 90°/180° spectrometer.[14] The spectrometer employed a photocathode

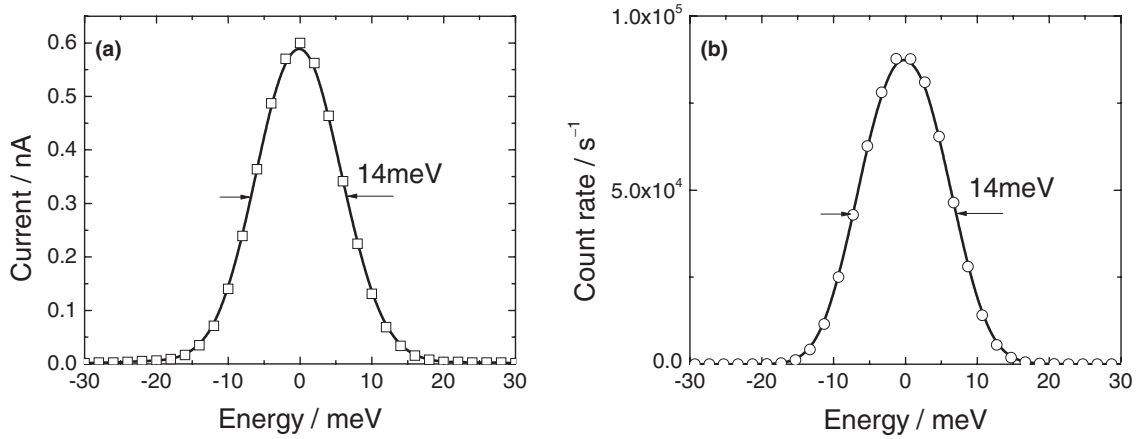

FIG. 8. Currents at the detector entrance (a) in direct beam and (b) after reflection from Cu(100). Unlike before (Fig. 4) there is no visible degradation of the resolution after reflection from the surface. The impact energy is 7.8 eV and the angle of incidence is 45°. The deflection voltages of monochromators and both analyzers are 3.0 V. The deflection voltage for the first monochromator is 4.5 V.

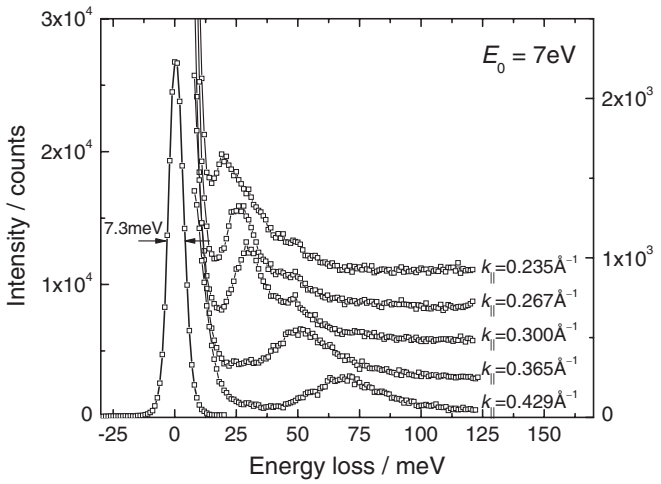

FIG. 9. Energy loss spectra of surface spin waves on an eight monolayer cobalt film deposited on a Cu(100) surface. The wave vector transfer is along the [110]-direction ($\bar{\Gamma}\,\bar{X}$-direction). The spin wave spectra refer to the right hand scale and are offset along the vertical axis. The impact energy on the sample is $E_0 = 7$ eV. The elastic diffuse line has a FWHM of 7.3 meV.

as spin-polarized source and the spectra were measured by the spin-asymmetry as function of energy loss. Due to the limited resolution ($\Delta E = 40$ meV (Refs. 6 and 19)) spin waves could be seen only for wave vectors larger than 0.35–0.4 Å^{-1}. Here we show data for the same system and surface direction obtained with the new instrument (Fig. 9). The deflection voltages were 2 V and 1.5 V on the first and second monochromator and 2 V on the analyzers. The calculated energy resolution for these deflection voltages (see considerations above) is $\Delta E = 7.5$ meV in agreement with the experimental result (Fig. 9). The impact energy on the sample is $E_0 = 7$ eV. The angle between the initial $\boldsymbol{k}$-vector $\boldsymbol{k}^{(\mathrm{i})}$ and the final $\boldsymbol{k}$-vector $\boldsymbol{k}^{(\mathrm{f})}$ is kept constant at 90°. The wave vector transfer parallel to the surface $\Delta k_{||} = k_{||}^{(\mathrm{f})} - k_{||}^{(\mathrm{i})}$ is achieved by rotating the sample around the axis vertical to the scattering plane. Figure 9 shows a selection of spectra for wave vectors ranging from $k_{\|} = 0.233$ Å^{-1} to 0.426 Å^{-1}. Due to the five times higher resolution compared to the previous study the spin waves are seen as separate peaks even down to $k_{\|}$-vectors of 0.23 Å^{-1} and energies of 20 meV without the need for probing the spin-asymmetry or resorting to unfolding procedures. Further details of the experiment will be published in a forthcoming publication.[20]

VII. CONCLUDING REMARKS AND OUTLOOK

We have realized a new, high-intensity spectrometer which is specifically designed for studies of weak electronic energy losses such as surface spin waves. The degradation of the resolution in studies of diffuse scattering events at low impact energies can be avoided by reducing the aberration for the β-angles of the 143°-deflector (at the expense of larger aberrations for the α-angles) in combination with an aperture for the α-angles. We have realized a spectrometer with the reduced β-aberrations in the analyzer by shifting the entrance and exit slits in the second analyzer to a larger radial position.

While the spectrometer is superior over previous designs with respect to intensity/resolution in the diffuse scattering regime it does not represent the technical optimum for two reasons. First, the resolution in the diffuse scattering regime should improve further without a loss of intensity by designing the first analyzer the same way as the second, hence with low aberrations for the β-angles. We abstained from such attempts since they would have entailed a complete remanufacturing of the entire analyzer part of the spectrometer. Second, the spectrometer is so far only optimized with respect to the monochromatic current and, within the limits described above, with respect to the resolution in the diffuse scattering regime. The intensity of a peak in the spectrum depends however also on the solid angle that is accepted by the lens/analyzer section of the spectrometer.

Previous studies have assumed that the acceptance angles for diffuse scattering from the target can be calculated from the acceptance angles of the analyzer in combination with phase space conservation rules[16] (see also Sec. 3.1 of Ref. 21). However, the applicability of this rule requires that an intermediate image of the monochromator exit slit is formed at the target which in turn is imaged onto the entrance slit of the analyzer. Extensive studies of the electron trajectories in the lens system showed however that this is not the case for the lens potentials that lead to maximum intensity of diffuse scattering. Rather, the lens potentials for diffuse scattering are approximately those in which a focus at the target exists with respect to the α-angles while a parallel beam is formed with respect to the β-angles. Experiments have shown that the diffuse scattering intensity is further improved by using different potentials for the analyzer and monochromator lens. Under such circumstances a calculation of the solid angle that is accepted by the lens/analyzer combination requires a complete simulation of the electron trajectories from the monochromator exit up to the channeltron entrance with an intermediate diffuse scattering at the target. Such calculations are under way and will be reported at a later time if they open the possibility for significant further improvements.

ACKNOWLEDGMENTS

The authors gratefully acknowledge the able technical support by Bernd Küpper during all stages of the development of the experimental equipment as well as the efforts of Lutz Baumgarten in the design of the experimental set-up. One of us (J.R.) expresses her sincere gratefulness to the NRW Research School "Forschung mit Synchrotronstrahlung in den Nano- und Biowissenschaften" for financial support. The authors are indebted to K. Zakeri for describing experimental details, in particular the potential setting used in Ref. 9 and for helpful discussions.

[1] H. Ibach and D. L. Mills, *Electron Energy Loss Spectroscopy and Surface Vibrations* (Academic, New York, 1982).
[2] K.-D. Tsuei, E. W. Plummer, A. Liebsch, E. Pehlke, K. Kempa, and P. Bakshi, Surf. Sci. **247**, 302 (1991).
[3] F. Moresco, M. Rocca, T. Hildebrandt, and M. Henzler, Phys. Rev. Lett. **83**, 2238 (1999).
[4] E. P. Rugeramigabo, T. Nagao, and H. Pfnür, Phys. Rev. B **78**, 155402 (2008).

[5]K. Pohl, B. Diaconescu, G. Vercelli, L. Vattuone, V. M. Silkin, E. V. Chulkov, P. M. Echenique, and M. Rocca, Eur. Phys. Lett. **90**, 57006 (2010).
[6]R. Vollmer, M. Etzkorn, P. S. A. Kumar, H. Ibach, and J. Kirschner, Phys. Rev. Lett. **91**, 147201 (2003).
[7]Y. Zhang, P. A. Ignatiev, J. Prokop, I. Tudosa, T. R. F. Peixoto, W. X. Tang, K. Zakeri, V. S. Stepanyuk, and J. Kirschner, Phys. Rev. Lett. **106**, 127201 (2011).
[8]Y. Zhang, P. Buczek, L. Sandratskii, W. X. Tang, J. Prokop, I. Tudosa, T. R. F. Peixoto, K. Zakeri, and J. Kirschner, Phys. Rev. B **81**, 094438 (2010).
[9]K. Zakeri, Y. Zhang, J. Prokop, T. H. Chaung, N. Sakr, W. X. Tang, and J. Kirschner, Phys. Rev. Lett. **104**, 137203 (2010).
[10]W. X. Tang, Y. Zhang, I. Tudosa, J. Prokop, M. Etzkorn, and J. Kirschner, Phys. Rev. Lett. **99**, 087202 (2007).
[11]H. Ibach, *Physics of Surfaces and Interfaces* (Springer, Berlin, 2006).
[12]H. Ibach, J. Electron Spectrosc. Relat. Phenom. **64/65**, 819 (1993).
[13]H. Ibach, M. Balden, and S. Lehwald, J. Chem. Soc., Faraday Trans. **92**, 4771 (1996).
[14]H. Ibach, D. Bruchmann, R. Vollmer, M. Etzkorn, P. S. A. Kumar, and J. Kirschner, Rev. Sci. Instrum. **74**, 4089 (2003).
[15]H. Ibach, M. Etzkorn, and J. Kirschner, Surf. Interface Anal. **38**, 1615 (2006).
[16]H. Ibach, *Electron Energy Loss Spectrometers—The Technology of High Performance* (Springer, Berlin, 1991).
[17]K. Zakeri, private communication (April, 2011).
[18]We thank K. Zakeri for providing the potential settings.
[19]M. Etzkorn, P. S. Anil Kumar, R. Vollmer, H. Ibach, and J. Kirschner, Surf. Sci. **566–568**, 241 (2004).
[20]J. Rajeswari, H. Ibach, C. M. Schneider, A. T. Costa, and D. L. Mills, "Electron energy loss spectroscopy of surface spin waves and phonons of fcc cobalt films on Cu(100)" (to be published).
[21]M. Etzkorn, Thesis Martin-Luther University Halle-Wittenberg, Halle 2005, urn:nbn:de:gbv:3-000008590.